Electronic Supplementary Material (ESI) for Journal of Materials Chemistry A.

Supporting Information for

Microstructural and Photoconversion Efficiency Enhancement of Compact Films of Lead-Free Perovskite Derivative $Rb_3Sb_2I_9$†

Fengzhu Li,[‡a] Yan Wang,[a] Kai Xia,[a] Robert L. Z. Hoye,[b] Vincenzo Pecunia[‡a*]

[a] Institute of Functional Nano & Soft Materials (FUNSOM), Jiangsu Key Laboratory for Carbon-Based Functional Materials & Devices, Soochow University, 199 Ren'ai Road, Suzhou, 215123, Jiangsu, PR China. E-mail: vp293@suda.edu.cn

[b] Department of Materials, Imperial College London, Exhibition Road, London SW7 2AZ, United Kingdom.

‡ F. L. and V. P. contributed equally to this work.

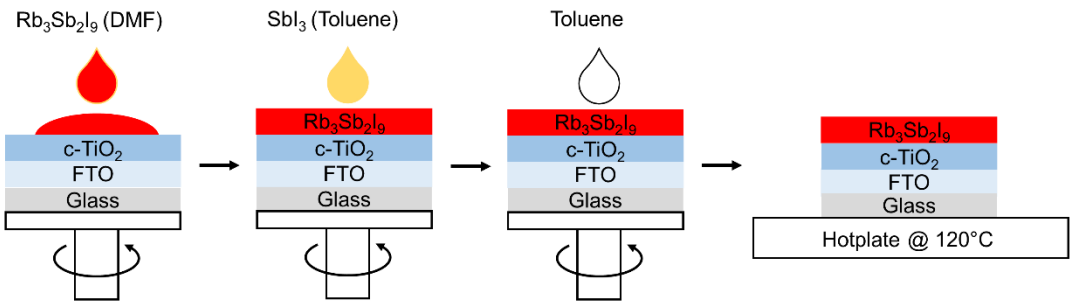

Figure S1 Conventional process (CP) referred to in the main text for the deposition of $Rb_3Sb_2I_9$ films. Here, antisolvent processing is carried out in two steps: firstly by dripping a dilute SbI_3 solution in toluene to compensate for iodine deficiency (*SbI_3:toluene dripping*), and then by dripping pure toluene to remove any excess SbI_3 (*toluene washing*). This is followed by a simple hotplate annealing.

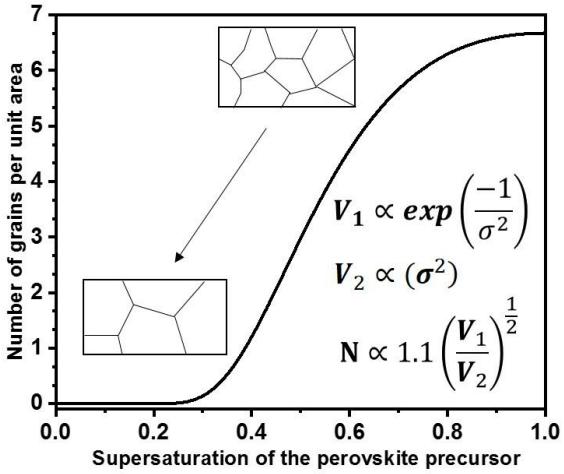

Figure S2 Relationship between grain size and supersaturation. V_1: crystal nucleation rate; V_2: crystal growth rate; σ: supersaturation level of the perovskite precursor; N: number of grains per unit area.[1] In nucleation theory,[2] the nucleation rate (V_1) is an exponential function of the supersaturation level (σ). On the other hand, according to the Burton-Cabrera-Frank (BCF) theory[3] at the low supersaturation levels, the crystal growth rate is a square function of the supersaturation level (σ). The resulting number of grains per unit area (N) reflects the combined effect of V_1 and V_2.

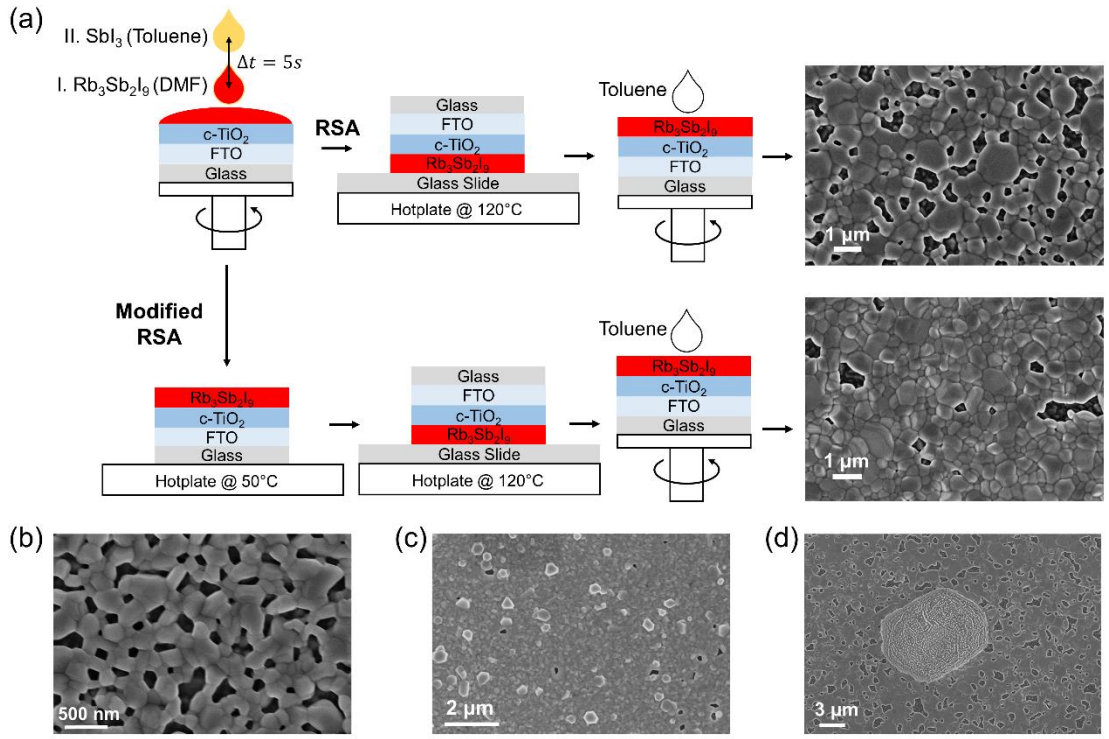

Figure S3 Basic RSA and modified RSA. (a) Schematic depiction of basic RSA and modified RSA, and SEM images of the resulting films. As discussed in the main text, the two types of RSA build on CP, differing from the latter mainly in regard to the hotplate annealing step, which is conducted with the sample turned over onto a glass slide so as to reduce the solvent evaporation rate. In addition, modified RSA features a straightforward hotplate annealing step at 50 °C prior to RSA proper, so as to limit the amount of solvent available when the sample is finally capped. We note that the glass substrates used for capping during RSA/modified RSA do not stick to the $Rb_3Sb_2I_9$ films. (b) SEM image of a film obtained when antisolvent processing in RSA is carried out as in CP (sequential *SbI_3:toluene dripping* and *toluene washing*): small domains and a large number of pinholes are formed. This can be attributed to the large amount of antisolvent left in the film during the annealing step, which disturbs grain growth. (c) SEM image of a film obtained when no antisolvent processing is carried out in RSA: small domains are formed, as likely determined by iodine deficiency. (d) SEM image of a large crystal-like feature on the film surface, obtained when RSA is conducted with only *SbI_3:toluene dripping* but no *toluene washing*. Features such as this come along with nearly pinhole-free films and large domain size. Such features, however, can be easily removed by dripping pure toluene *after* the annealing step of RSA, which leads to the modified RSA process flow shown in (a).

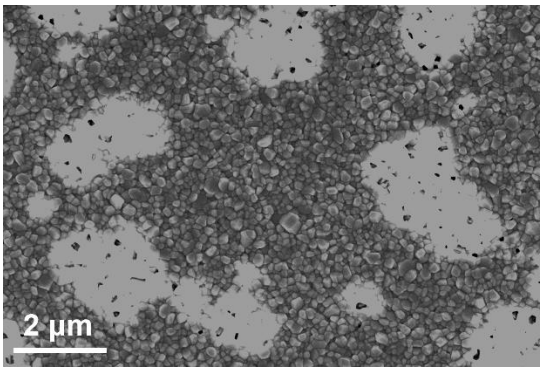

Figure S4 SEM images of film obtained via 225°C annealing without SbI_3 vapor assisted.

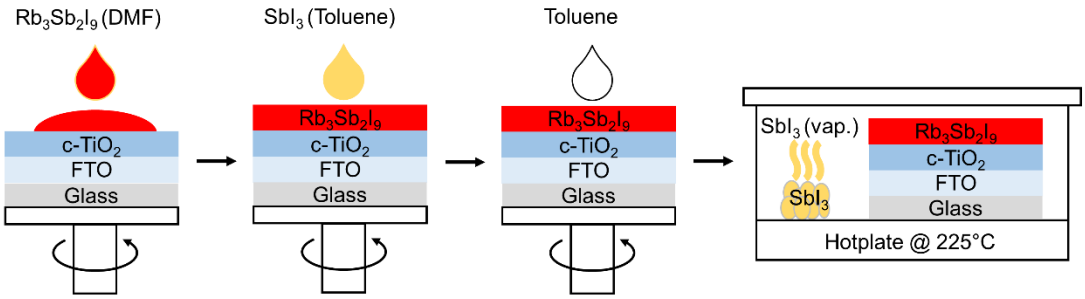

Figure S5 Schematic depiction of the HTVA process flow.

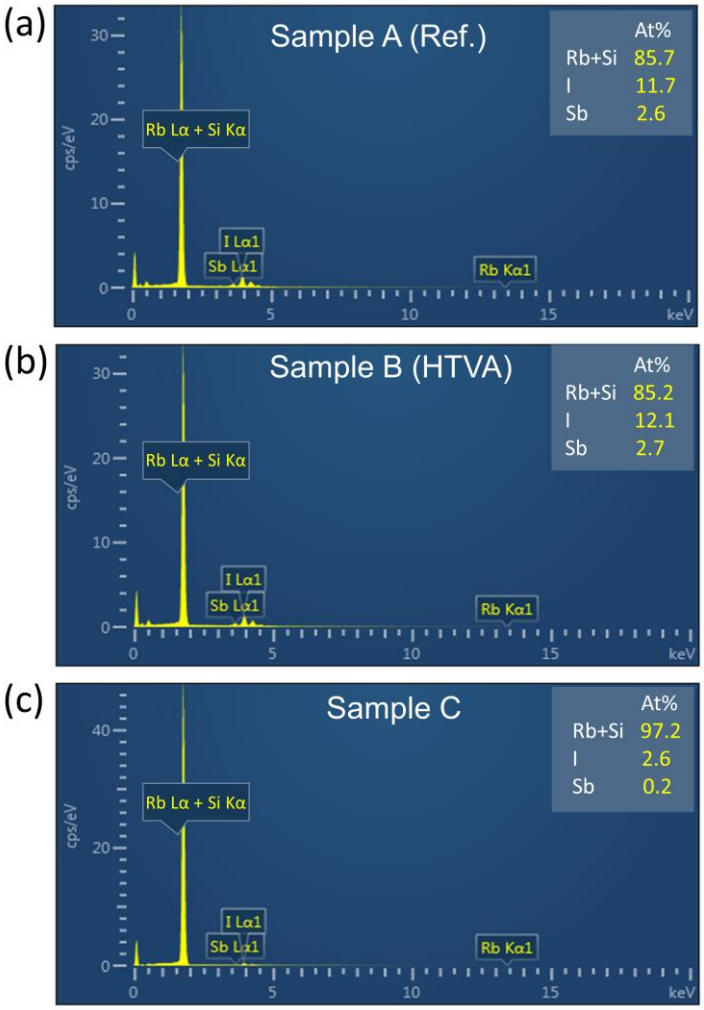

Figure S6 Energy-dispersive X-ray spectroscopy (EDS) of films processed through different methods. (a) Reference sample processed via CP and not subjected to high-temperature annealing (Sample A). (b) Sample annealed at 225 °C in SbI_3 vapor (HTVA; Sample B). (c) Sample annealed at 225 °C but not exposed to SbI_3 vapor (Sample C). All samples were fabricated on Silicon substrates.

Table S1 Values of the Sb/I ratio measured by EDS from the samples presented in Figure S6.

	Sb/I ratio
Sample A (reference)	0.222
Sample B (HTVA)	0.223
Sample C	0.077
Expected	0.222

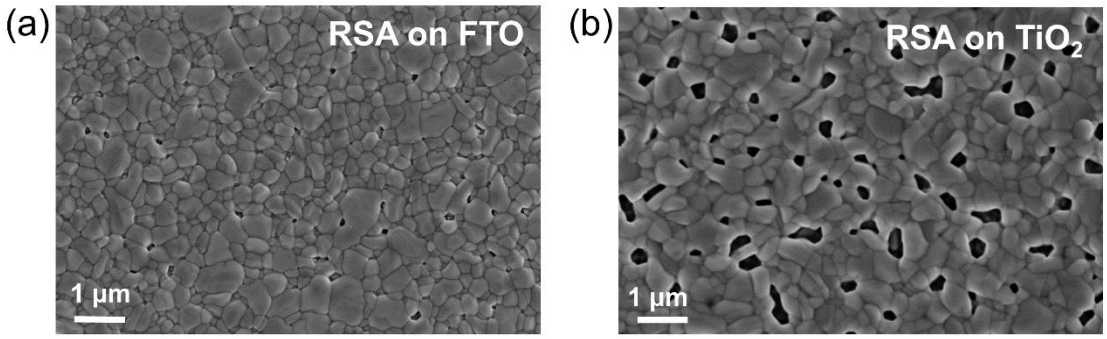

Figure S7 SEM images of RSA films on (a) FTO- and on (b) TiO_2-coated substrates.

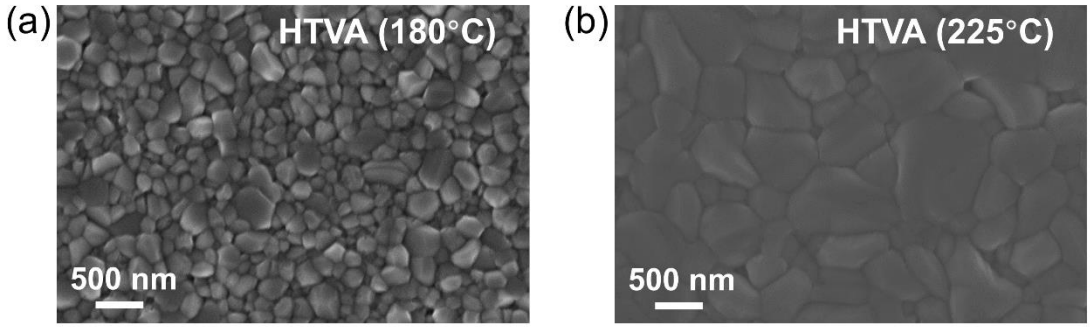

Figure S8 SEM images of films obtained via HTVA (a) at 180 °C and (b) at 225 °C.

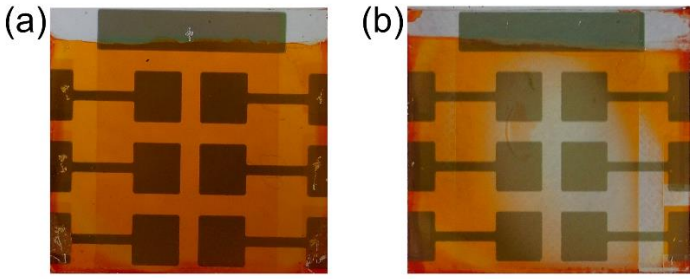

Figure S9 Photographs of samples in which $Rb_3Sb_2I_9$ was processed via HTVA at different annealing temperatures: (a) 225 °C; (b) 250 °C.

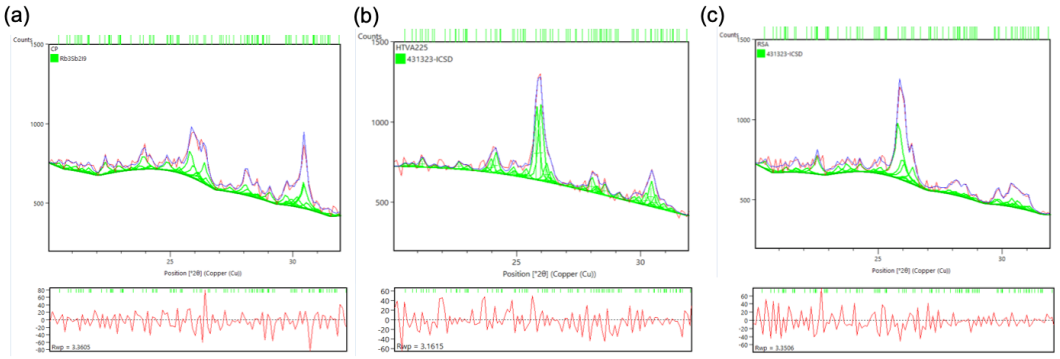

Figure S10. Diffraction patterns of $Rb_3Sb_2I_9$ films grown by the (a) conventional process, (b) high-temperature vapor annealing and (c) reduced supersaturation annealing methods. The patterns were fit using Pawley's method and the residuals are shown below.

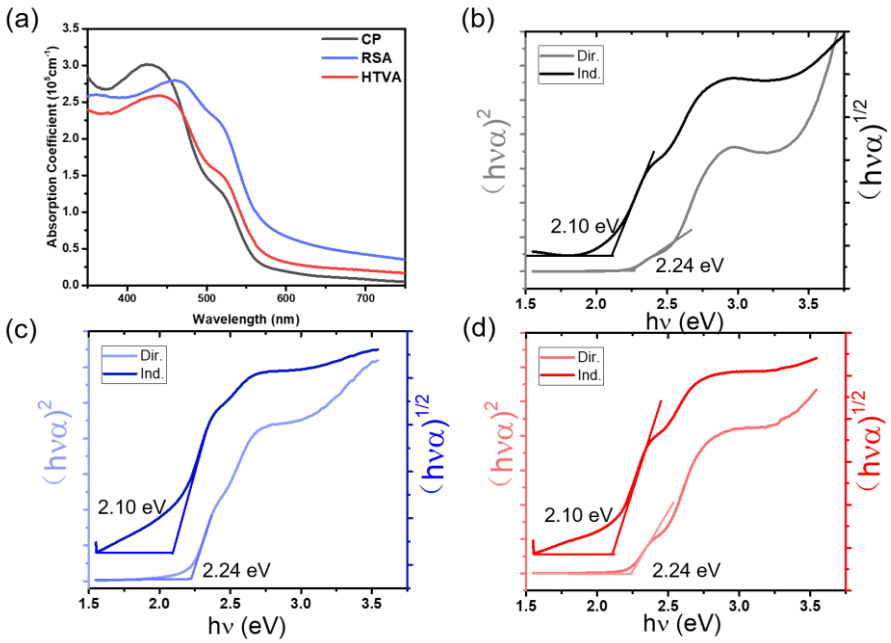

Figure S11 (a) Absorption coefficient of CP, RSA, HTVA films determined from absorbance data. Tauc plots of $Rb_3Sb_2I_9$ films deposited by (b) CP, (c) RSA, and (d) HTVA.

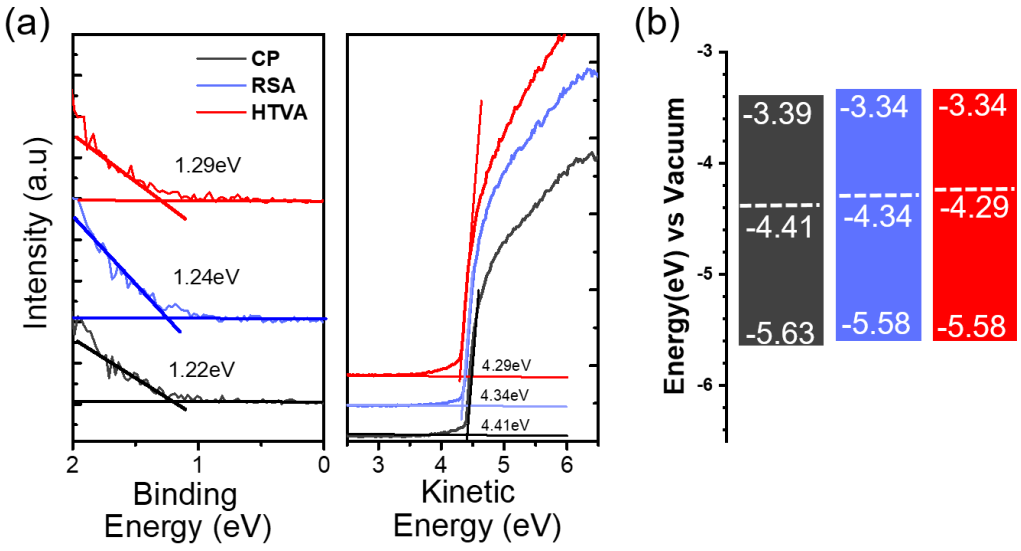

Figure S12 (a) UPS intensity from $Rb_3Sb_2I_9$ films: valence band states (left) and He I secondary electron cutoff (right). (b) Energy level diagrams derived from UPS and UV-Vis absorption data, under the approximation of negligible excitonic effects.

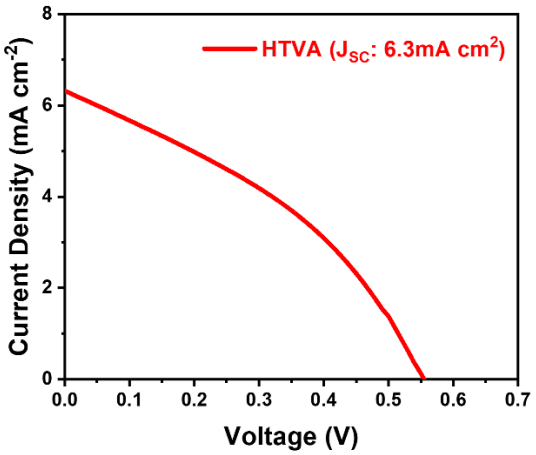

Figure S13 Measured current–voltage characteristic of a HTVA $Rb_3Sb_2I_9$ devices giving a short-circuit current density of 6.3 mA cm^{-2} under AM1.5G illumination.

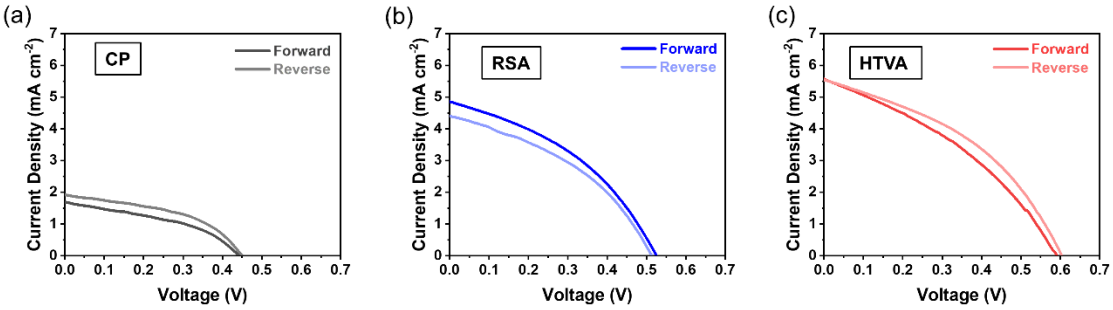

Figure S14 Double-sweep current–voltage characteristics of $Rb_3Sb_2I_9$ devices under AM1.5G illumination: (a) CP (H_{index} = 0.225); (b) RSA (H_{index} = -0.108); (c) HTVA (H_{index} = 0.126). The hysteresis index H_{index} is calculated as ($PCE_{Reverse}$ - $PCE_{Forward}$)/$PCE_{Reverse}$.[4]

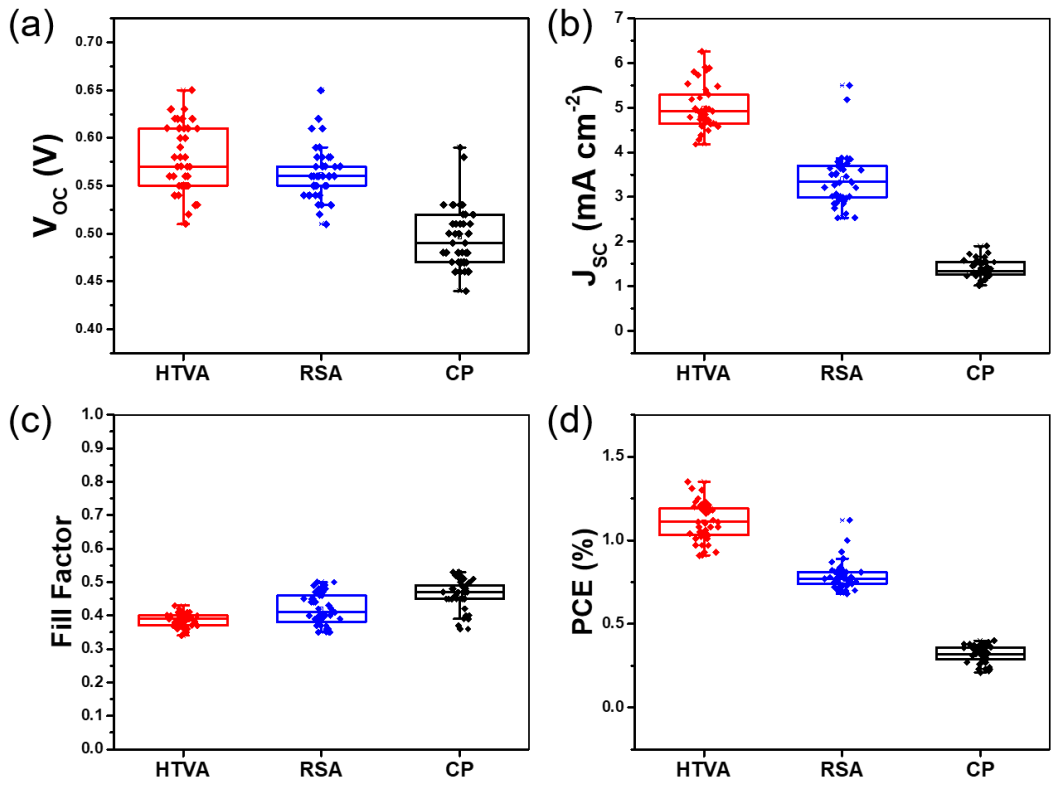

Figure S15 Photovoltaic parameter distribution of the different types of $Rb_3Sb_2I_9$ devices investigated in this work (40 devices of each sample type): (a) V_{oc}; (b) J_{sc}; (c) Fill Factor; (d) PCE.

Table S2 Performance of solar cells based on Bi- and Sb-halide perovskite derivatives (i.e., $A_3M_2X_9$, A^+: organic/inorganic cation, M: Sb^{3+}/Bi^{3+}, X^-: halide anion) from the literature.

Active layer	Device Structure	V_{oc} (V)	J_{sc} (mA cm^{-2})	FF (%)	PCE (%)	EQE_{max} (%)	Ref
$MA_3Bi_2I_9$	inverse	0.83	1.39	34	0.39	23	[5]
$MA_3Bi_2I_9$	mesoporous	1.01	4.02	78	3.17	48	[6]
$MA_3Bi_2I_9$	mesoporous	0.67	1.00	60	0.42	25	[7]
$MA_3Bi_2I_9$	mesoporous	0.65	1.1	50	0.36	No data	[8]
$MA_3Bi_2I_9$	mesoporous	0.51	0.94	61	0.31	28	[9]
$MA_3Bi_2I_9$	mesoporous	0.56	0.83	49	0.26	4.6	[10]
$MA_3Bi_2I_9$	mesoporous	0.68	0.52	33	0.12	12	[11]
$MA_3Bi_2I_9$	regular	0.72	0.49	32	0.11	17	[12]
$MA_3Bi_2I_9$	mesoporous	0.35	1.16	0.46	0.19	22	[13]
$MA_3Bi_2I_9$	inverse	0.66	0.22	0.49	0.07	No data	[14]
$MA_3Bi_2I_9$	mesoporous	0.84	0.17	35	0.05	4.0	[15]
$MA_3Bi_2I_9$	mesoporous	0.83	3.00	79	1.64	60	[16]
$MA_3Bi_2I_9$	mesoporous	0.87	2.7	69	1.62	25	[17]
$C_5H_6NBiI_4$	mesoporous	0.62	2.71	54	0.9	No data	[18]
$(C_6H_5NH_3)BiI_4$	mesoporous	0.58	6.03	22	0.78	No data	[19]
$Cs_3Bi_2I_9$	mesoporous	0.31	3.4	38	0.4	25	[20]
$Cs_3Bi_2I_9$	mesoporous	0.85	2.15	60	1.09	37	[11]
$Cs_3Bi_2I_9$	regular	0.86	5.78	64	3.2	56	[21]
$MA_3Sb_2I_9$	inverse	0.90	1.00	55	0.49	13	[22]
$MA_3Sb_2I_9$	inverse	0.62	5.41	61	2.04	21	[23]
$MA_3Sb_2I_9$	inverse	0.70	6.64	60	2.77	26	[24]
$Cs_3Sb_2I_9$	inverse	0.60	2.91	48	0.84	18	[23]
$Cs_3Sb_2I_9$	inverse	0.68	5.31	39	1.49	39	[25]

References

1 D. Liu, W. Zhou, H. Tang, P. Fu and Z. Ning, *Sci. China Chem.*, 2018, **61**, 1278–1284.

2 A. E. Nielsen, *Kinetics of precipitation*, Pergamon, 1964, vol. 18.

3 W.-K. Burton, N. Cabrera and F. C. Frank, *Philos. Trans. R. Soc. London. Ser. A, Math. Phys. Sci.*, 1951, **243**, 299–358.

4 Q. Jiang, Y. Zhao, X. Zhang, X. Yang, Y. Chen, Z. Chu, Q. Ye, X. Li, Z. Yin and J. You, *Nat. Photonics*, 2019, **13**, 460–466.

5 C. Ran, Z. Wu, J. Xi, F. Yuan, H. Dong, T. Lei, X. He and X. Hou, *J Phys Chem Lett*, 2017, **8**, 394–400.

6 S. M. Jain, D. Phuyal, M. L. Davies, M. Li, B. Philippe, C. De Castro, Z. Qiu, J. Kim, T. Watson, W. C. Tsoi, O. Karis, H. Rensmo, G. Boschloo, T. Edvinsson and J. R. Durrant, *Nano Energy*, 2018, **49**, 614–624.

7 X. Zhang, G. Wu, Z. Gu, B. Guo, W. Liu, S. Yang, T. Ye, C. Chen, W. Tu and H. Chen, *Nano Res.*, 2016, **9**, 2921–2930.

8 S. S. Mali, H. Kim, D.-H. Kim and C. Kook Hong, *ChemistrySelect*, 2017, **2**, 1578–1585.

9 A. Kulkarni, T. Singh, M. Ikegami and T. Miyasaka, *RSC Adv.*, 2017, **7**, 9456–9460.

10 T. Singh, A. Kulkarni, M. Ikegami and T. Miyasaka, *ACS Appl. Mater. Interfaces*, 2016, **8**, 14542–14547.

11 B. W. Park, B. Philippe, X. Zhang, H. Rensmo, G. Boschloo and E. M. Johansson, *Adv Mater*, 2015, **27**, 6806–6813.

12 M. Abulikemu, S. Ould-Chikh, X. Miao, E. Alarousu, B. Murali, G. O. Ngongang Ndjawa, J. Barbé, A. El Labban, A. Amassian and S. Del Gobbo, *J. Mater. Chem. A*, 2016, **4**, 12504–12515.

13 M. Lyu, J.-H. Yun, M. Cai, Y. Jiao, P. V Bernhardt, M. Zhang, Q. Wang, A. Du, H. Wang, G. Liu and L. Wang, *Nano Res.*, 2016, **9**, 692–702.

14 S. Öz, J.-C. Hebig, E. Jung, T. Singh, A. Lepcha, S. Olthof, F. Jan, Y. Gao, R. German, P. H. M. van Loosdrecht, K. Meerholz, T. Kirchartz and S. Mathur, *Sol. Energy Mater. Sol. Cells*, 2016, **158**, 195–201.

15 H. Li, C. Wu, Y. Yan, B. Chi, J. Pu, J. Li and S. Priya, *ChemSusChem*, 2017, **10**, 3994–3998.

16 Z. Zhang, X. Li, X. Xia, Z. Wang, Z. Huang, B. Lei and Y. Gao, *J Phys Chem Lett*, 2017, **8**, 4300–4307.

17 S. M. Jain, T. Edvinsson and J. R. Durrant, *Commun. Chem.*, , DOI:10.1038/s42004-019-0195-3.

18 T. Li, Y. Hu, C. A. Morrison, W. Wu, H. Han and N. Robertson, *Sustain. Energy Fuels*, 2017, **1**, 308–316.

19 X.-L. Li, L.-L. Gao, B. Ding, Q.-Q. Chu, Z. Li and G.-J. Yang, *J. Mater. Chem. A*, 2019, **7**, 15722–15730.

20 M. B. Johansson, H. Zhu and E. M. Johansson, *J Phys Chem Lett*, 2016, **7**, 3467–3471.

21 F. Bai, Y. Hu, Y. Hu, T. Qiu, X. Miao and S. Zhang, *Sol. Energy Mater. Sol. Cells*, 2018, **184**, 15–21.

22 J.-C. Hebig, I. Kühn, J. Flohre and T. Kirchartz, *ACS Energy Lett.*, 2016, **1**, 309–314.

23 K. M. Boopathi, P. Karuppuswamy, A. Singh, C. Hanmandlu, L. Lin, S. A. Abbas, C. C. Chang, P. C. Wang, G. Li and C. W. Chu, *J. Mater. Chem. A*, 2017, **5**, 20843–20850.

24 P. Karuppuswamy, K. M. Boopathi, A. Mohapatra, H.-C. Chen, K.-T. Wong, P.-C. Wang and C.-W. Chu, *Nano Energy*, 2018, **45**, 330–336.

25 A. Singh, K. M. Boopathi, A. Mohapatra, Y. F. Chen, G. Li and C. W. Chu, *ACS Appl Mater Interfaces*, 2018, **10**, 2566–2573.